RSC Advances

ROYAL SOCIETY OF CHEMISTRY

PAPER

View Article Online
View Journal | View Issue

Check for updates

Cite this: *RSC Adv.*, 2023, **13**, 33852

Catalytic upgrading of volatiles in co-pyrolysis of coal and biomass by Mo-MFI molecular sieves

Qiuli Zhang, *[a] Shuo Zhang,[a] Junli Liu,[b] Jingjing Li,[a] Jiahui Liu,[a] Jun Zhou[a] and Lei Wu[a]

Received 12th October 2023
Accepted 14th November 2023

DOI: 10.1039/d3ra06925g

rsc.li/rsc-advances

Catalytic co-pyrolysis of coal and biomass can improve both solid waste utilization and high value-added product content to obtain higher quality oils, which is significant for the clean and efficient use of coal and the expansion of biomass resource utilization. This study focuses on improving the quality of tar and the content of light fractions by catalytic reforming of coal and biomass co-pyrolysis volatiles. Molybdenum-doped MFI-type molecular sieve catalysts (Mo-MFI) were successfully prepared by a hydrothermal method using TPAOH as a structure-directing agent. The synthesized Mo-MFI molecular sieves were then used in the catalytic reforming of volatile fractions from the co-pyrolysis of low-metamorphic coal and biomass. With the help of biomass and catalyst, the co-pyrolysis tar can increase the content of high-value-added products. It was found that the highest tar yield of 11.4% was achieved when 30 wt% of corn stover was added. The utilization of Mo-MFI catalysts leads to a significant increase of 126% in the light oil content of a blended sample tar consisting of 30 wt% corn stover. The catalyst was also highly selective for low-level phenols, increasing the phenol content in the co-pyrolysis tar by 133.8%, 112.2% for cresols, and 88.1% for xylenol. In addition, a possible reaction pathway for the conversion of hydrocarbons to PXC (phenol, cresol, and xylenol) was proposed based on the changes in the components of the tar product after the addition of the catalyst.

1. Introduction

China has abundant and widely distributed reserves of coal, with low metamorphic coal accounting for over 55% of the total reserves.[1] Coal pyrolysis is a crucial stage in the processing and utilization of coal.[2] Coal tar obtained through low-temperature pyrolysis typically contains 20–30% phenolic compounds, including high-value raw chemicals (phenol, cresol, and xylenol, referred to as PCX). These compounds are widely used in the production of synthetic resins, plant protectants, preservatives, coatings, pesticides, antioxidants, and other chemical products.[3] However, the recombinant fractions in coal tar are difficult to separate. Therefore, further processing is required to produce fuels and chemicals.[4–6] Catalytic reforming of gaseous tar produced during coal pyrolysis is an efficient method to enhance the quality of tar and increase the yield of lighter fractions.

Biomass, which is a promising renewable energy source with high H/C and O/C ratios, exhibits synergistic effects when co-pyrolyzed with coal.[7] This interaction between coal and biomass pyrolysis components can improve the utilization value of pyrolysis products. Co-pyrolysis can not only solve the pollution problems caused by the combustion and disposal of biomass waste but also improve the efficiency of coal conversion and obtain higher-quality oil products. Meanwhile, the partial replacement of coal by biomass can effectively reduce the emission of pollutants, alleviate the energy crisis and environmental pollution caused by the utilization of fossil fuels, and promote the sustainable development of the energy system and the benign circle of the ecological environment.[8–10]

Catalytic pyrolysis offers several advantages over simple pyrolysis, including reduced energy consumption, enrichment of target products, and optimized product molecular weight distribution. Zeolite molecular sieves with MFI-type topology are one of the most commonly used catalyst types due to their tunable surface acidity, shape-selective catalysis, and excellent hydrothermal stability. They are an ideal carrier for metal-laden active centers and play a crucial role in various catalytic hydrocarbon conversion processes such as petroleum refining, chemical manufacturing, coal conversion, and environmental catalysis.[11,12] Typically, the pore structure and acidity of molecular sieves are the main factors affecting the catalytic activity, which is hindered by the restricted access of some larger reactant molecules to the internal catalytic centre through the micropores. In order to enhance the catalytic performance of molecular sieves, researchers generally modify their acidic and ion-exchange properties by constructing hierarchical pore structures or doping

---

[a] *School of Chemistry and Chemical Engineering, Xi'an University of Architecture and Technology, Xi'an, 710055, China. E-mail: qiulizhang@126.com*

[b] *Shenmu Sanjiang Coal Chemical Co., Ltd., Shenmu Economic and Technological Development Zones, Shenmu, 719300, China*

elements with different oxidation states and electronegativity.[13] Previously, MFI catalysts were mostly used for upgrading monocyclic aromatic hydrocarbons and lightweight olefins in coal pyrolysis tars. For example, Bi *et al.* applied Ga loading on MFI for the catalytic upgrading of coal volatiles and improved the conversion of aliphatic and polycyclic aromatic hydrocarbons to BTEXN (benzene, toluene, ethylbenzene, xylene, naphthalene) in tar.[14] Yang *et al.* used Mo-modified MFI catalysts for the pyrolysis of cellulose and found that the introduction of Mo not only suppressed the production of polyaromatic hydrocarbons and coke but also improved the product toluene selectivity in the products.[15] In previous studies, Mo was widely used in most catalytic reactions due to its excellent metal activity, such as ring-opening reactions of aromatic and cycloalkanes, hydrocracking and aromatization of alkanes.[16–18]

In recent years, researchers have conducted a lot of research on the coal pyrolysis process, and the research content in the pyrolysis mode mainly focuses on the two parts of synergistic pyrolysis of coal with other substances or catalytic pyrolysis of coal.[19–22] To our knowledge, the application of Mo-modified MFI in the catalytic reforming of volatiles from the co-pyrolysis of low metamorphic coal and biomass has not been reported yet. Therefore, this study aimed to enrich the light fraction in the co-pyrolysis of coal and biomass by introducing Mo-doped MFI. The catalyst used was a Mo-doped MFI-type molecular sieve (Mo-MFI) synthesized by hydrothermal method. This synthesis method addressed issues such as the non-uniform distribution of metals on the carrier and the easy agglomeration of metals. This study achieved the goal of enriching lighter components through the synergistic effect of biomass and Mo-MFI catalysts. Mo-MFI has high selectivity for low-level phenols and reduces the heavy fraction in co-pyrolysis tars, thus enhancing the value of the oil.

2. Experimental section

2.1 Materials and reagents

Tetraethyl orthosilicate (TEOS, 98%), tetrapropylammonium hydroxide (TPAOH, 25%) were obtained from Shanghai Yi En Chemical Technology Co., Ltd. Ammonium molybdate tetrahydrate ($(NH_4)_6Mo_7O_{24}\cdot 4H_2O$), and aqueous ammonia ($NH_4OH$, 25%) were obtained from Sinopharm Chemical Reagent Co. All solvents and chemicals were obtained from cally pure and used without further purification.

The raw materials for this study were low metamorphic coal (C) and corn stover (B), where the low metamorphic coal came from the Zhangjiamao area and the corn straw from a feed mill, which were dried by natural ventilation for 48 h. The research samples were crushed and sieved to obtain particle sizes of 150 mesh to 200 mesh and placed in a desiccator for backup. The results of both industrial and elemental analyses of both are shown in Table 1.

Table 1 Proximate and ultimate analyses of low metamorphic coal and corn stover[a]

	Proximate analysis (%)				Ultimate analysis (%)				
	M_{ad}	A_{ad}	V_{ad}	FC_{ad}	C_{daf}	H_{daf}	O_{daf}	N_{daf}	S_{daf}
C	6.61	4.96	33.35	55.08	79.10	5.04	14.27	1.08	0.51
B	8.70	1.51	83.17	6.62	47.31	4.57	47.05	1.04	0.03

[a] M (moisture), A (ash), V (volatile), FC (fixed carbon); ad (measured in air-dry base condition); daf (measured in a dry, ash-free state); O_{daf} (oxygen content is calculated by difference).

2.2 Preparation of catalyst

Synthesis of silicalite-1 nanocrystalline seeds. Mix 4.5 mL of TPAOH with 5 mL of TEOS and stir vigorously at room temperature for 1 hour. Afterward, add H_2O and continue stirring for an additional 2 hours (without evaporation the alcohol following hydrolyzing the TEOS). The molar composition ratio of this mixture was $1.0SiO_2$: 0.24 TPAOH: $24.2H_2O$. The obtained material was transferred into a Teflon-lined autoclave (100 mL) and put into a 170 °C oven for 48 h. After crystallization, the product was removed by natural cooling and centrifuged at 8000 rpm to obtain the solid product, which was washed with ethanol and deionized water until the filtrate was centered and dried overnight in an oven at 80 °C. The dried solid was thermally treated in the air at 550 °C for 6 h to remove the organic template agent.

Mo-MFI molecular sieve synthesis. To prepare the pure silicon molecular sieve silicalite-1 nanocrystalline species, a specific quantity of ammonium molybdate is dissolved in water until it is fully dissolved. Next, an ammonia solution is added to adjust the value of pH to 10. Afterward, an appropriate amount of pure silicon molecular sieve silicalite-1 nanocrystalline species is added to the system, and the system is sonicated to ensure uniform dispersion of the pure silicon molecular sieve. The molar composition ratio of this mixture was 1.0 SiO_2: $xMoO_3$: 0.24 TPAOH: $72.4H_2O$ ($x = 0.010$, 0.020, 0.030, and 0.040). The obtained material was transferred into a Teflon-lined autoclave (100 mL) and put into a 170 °C oven for 48 h. At the end of the period, the product was removed by natural cooling and centrifuged at 8000 rpm to obtain the solid product, which was washed with ethanol and deionized water until the filtrate was centered, and the product was dried overnight in an oven at 80 °C. The dried solid was thermally treated in the air at 550 °C for 6 h. The resulting molecular sieve was labeled as Si/Mo-*n*, where *n* represents the initial synthetic gel's Si/Mo molar ratio ($n = 25$, 33, 50, 100). For example, the Si/Mo-100 sample was composed of a gel composition of $1.0SiO_2$ and $0.010MoO_3$.

2.3 Experimental setup and method

The pyrolysis experimental device is shown in Fig. 1. The sample of coal and corn stover was crushed and sieved before the experiment. The resulting pellets with sizes ranging from approximately 0.4 mm to 0.6 mm were mixed thoroughly and placed in a porcelain boat. Subsequently, 5 g of the sample was separated from 1 g of catalyst using quartz wool and placed in a tube furnace. After expelling the air in the furnace by passing N_2, the furnace was heated from room temperature to 650 °C at a rate of 10 °C min^{-1} to complete the pyrolysis process. The collected liquid product was dehydrated and determined by GC-MS after

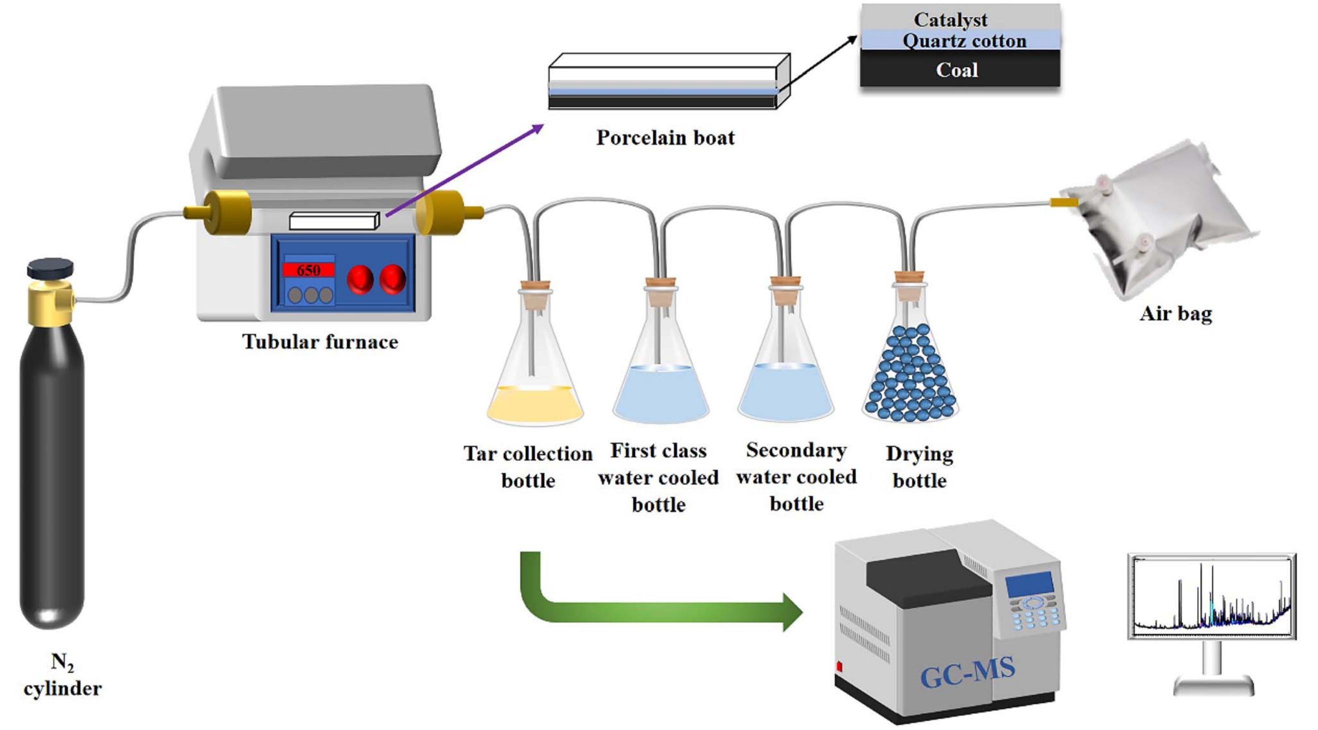

Fig. 1 Schematic diagram of pyrolysis system.

the co-pyrolysis experiment. After cooling to room temperature, the solid products were collected. To ensure the authenticity and reliability of the experimental data, each experiment was conducted three times and the average value was used as the final data to calculate the yield of pyrolysis products. The yield of pyrolysis products such as char, tar, pyrolysis water, and gas were calculated using the equations provided.

$$w_{\text{char}} = \frac{M_{\text{char}}}{M}$$

$$w_{\text{liquid}} = \frac{M_{\text{liquid}}}{M} = \frac{M_2 - M_1}{M}$$

$$w_{\text{tar}} = \frac{M_{\text{tar}}}{M}$$

$$w_{\text{water}} = w_{\text{liquid}} - w_{\text{tar}}$$

$$w_{\text{gas}} = 1 - w_{\text{liquid}} - w_{\text{char}}$$

where w_{char}, w_{liquid}, w_{tar}, w_{water}, w_{gas} are the yields of char, liquid product, tar, pyrolysis water, and gas, respectively, M_{char}, M_{liquid}, M_{tar} are the masses of char, liquid product, and tar at the end of the experiment, M is the mass of raw material, M_1 and M_2 are the total masses of liquid product collection bottles before and after the experiment respectively.

2.4 Experimental analysis methods

By the National Standard of the People's Republic of China (No. GB/T 30732-2014 and GB/T 31391-2015), coal and solid products underwent both industrial and ultimate analysis. Fourier transform infrared Spectrum (FT-IR) of catalysts and Gas Chromatography-Mass Spectrometry (GC-MS) of liquid products were performed using a TGA/DSC3+-Nicolet iS50-TRACE 1300 ISQ 7000 (USA). A GeminiSEM 500 (Germany) Scanning Electron Microscope (SEM) was used to characterize the particle size of the catalyst. Transmission Electron Microscope (TEM) experiments were performed using a Talos F200X instrument (China). The ethanol solution containing the catalyst was dropped onto a copper mesh grid and then analyzed by transmission electron microscopy. X-ray Diffraction (XRD) analysis was performed using a SmartLab (Japan) to acquire X-ray powder diffraction (XRD) patterns of the samples in the 2θ range from 5° to 40° with a scanning speed of 5° min^{-1}. N_2 physisorption was measured on a JW-BK200 (China) specific surface area analyzer, and the specific surface area (S_{BET}) of the samples was calculated using the Brunauer–Emmett–Teller (BET) model; the micropore volume (V_{micro}) was calculated using the Horvath–Kawazoe (HK) model; the mesopore volume (V_{meso}) was calculated using the Barret–Joyner–Halenda (BJH) model. The elemental Mo content was determined by Inductively Coupled Plasma Optical Emission Spectrometer (ICP-OES) using Agilent 5110 (USA). UV-visible absorption spectra (UV-vis) were performed on a UV-2500 scanning spectrophotometer (Japan).

3. Results and discussion

3.1 Characterization of catalysts

The XRD patterns of MFI-type molecular sieves with varying silicon-to-molybdenum ratios were almost the same as the pure silica Silicalite-1 molecular sieves (PDF44-0696), indicating that the prepared Mo-MFI possess high crystallinity and purity (Fig. 2a).[29] However, the diffraction peaks in the range of 22° to 25° in the XRD spectra of the samples are slightly shifted to a lower angle compared to the pure silicon Silicalite-1 molecular sieve, and this subtle XRD diffraction peak variation may be related to the distorted deformation of the molecular sieve skeleton caused by the replacement of Si atoms by Mo atoms with larger radius.[13] For Si/Mo-*n* ($n = 25, 33, 50, 100$) diffraction peaks split at approximately $2\theta = 23.4°$, 23.8° and 24.5° (the inset of Fig. 2a), indicating that a part of the molybdenum species has entered the skeleton of the MFI-type molecular sieve.[30] The N_2 adsorption–desorption isotherms of the pure silica Silicate-1 sample and various Si/Mo-*n* exhibited typical type I isotherms (Fig. 2b), indicating that the dominant pore structure in these samples is microporous.[31] At the lower relative pressure range ($P/P_0 < 0.1$), the adsorption of nitrogen rises sharply, indicating that these molecular sieve samples have typical microporous.[32] At the higher relative pressure range ($P/P_0 > 0.9$), the sharp rise in the adsorption/desorption curves of all Si/Mo-*n* samples can be attributed to the presence of particle stacking pores.[33]

Table 2 lists the structural parameters of Silicate-1 and various Si/Mo-*n* molecular sieves. The specific surface area and pore volume of various Si/Mo-*n* molecular sieves were slightly lower than that of Silicate-1. In Mo-MFI, Si/Mo-33 has the maximum specific surface area of 321.1 $m^2\ g^{-1}$ and the pore volume of 0.2125 $cm^3\ g^{-1}$, suggesting that some Mo may have entered the skeleton. This larger specific surface and pore volume could improve the possibility of large substrate molecules in the pyrolytic volatiles approaching the active site.[34] As the Mo content increased, there was a decrease in specific surface area and pore volume. This can be attributed to excess Mo in the form of MoO_3 blocking the pores.

The SEM results of Silicate-1 and Si/Mo-33 samples are presented in Fig. 3. Both samples exhibit ellipsoidal morphology and relatively smooth surfaces. Silicate-1 has a particle size range of 180 to 260 nm with an average grain size of 223 nm, while Si/Mo-33 has a particle size range of 200 to 300 nm with an average grain size of 255 nm. It is indicated that the introduction of the molybdenum element will have some effect on the morphology. The ionic radius of Mo (55 pm) is known to be larger than that of Si (40 pm), and the increase in grain size of Si/Mo-33 may be due to the doping of Mo at tetrahedral positions in the skeleton.[13]

The TEM images of Silicate-1 and Si/Mo-33 samples are shown in Fig. 4, it clearly showed that Silicate-1 and Si/Mo-33 molecular sieves have relatively smooth surfaces and ellipsoidal morphology, which is consistent with the results observed in SEM images (Fig. 4a and b). Fig. 4c shows the HRTEM images of the prepared Si/Mo-33, the lattice fringe spacing of 0.24 nm is observed on the surface of Si/Mo-33, this lattice spacing is in line with the diffraction of MoO_3 crystal (111) surface features and suggests that there is some MoO_3 present on the surface of Si/Mo-33.[35] The absence of significant MoO_3 cluster aggregation in the image area suggests that the introduced Mo species are highly dispersed within the molecular sieve.

Fig. 5 presents the FT-IR and UV-vis spectra of MFI-type molecular sieves with varying silicon-to-molybdenum ratios. As shown in Fig. 5a, absorption peaks at 450, 551, 801, 1105, and 1230 cm^{-1} are observed for each sample, which is consistent with the previously reported FT-IR spectra of MFI-type molecular sieves.[36] In addition to this, each sample also shows a distinct characteristic peak at 627 cm^{-1} which is the Mo–O–Mo deformation vibration, which indicates the presence of a portion of Mo in the form of MoO_3.[37] The UV-vis diffused reflectance spectra of various samples exhibited the same main absorption bonds (Fig. 5b). The absorption peak at 223 nm in

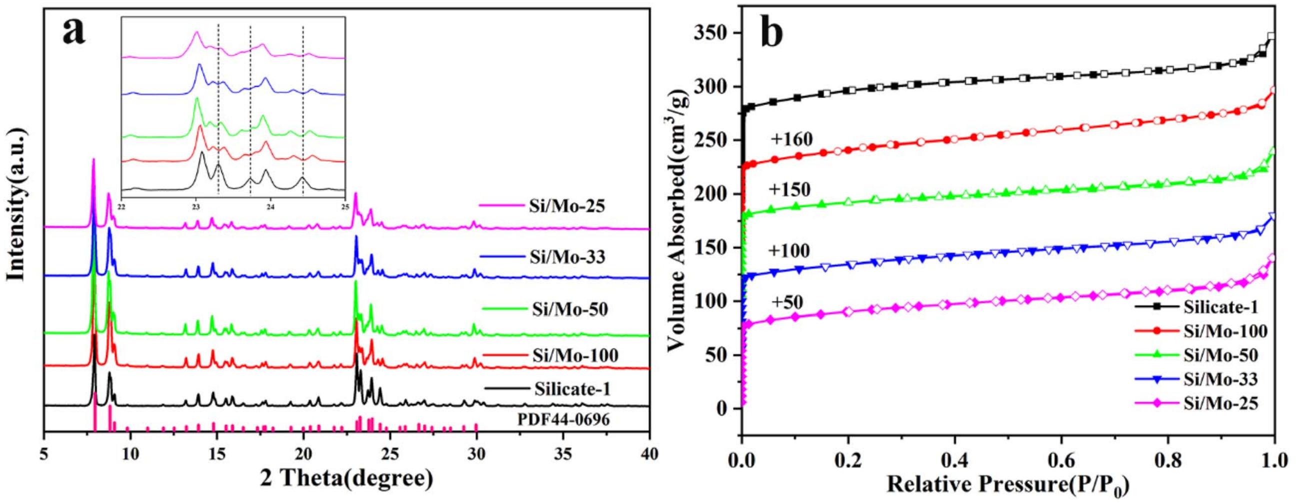

Fig. 2 XRD patterns of various Si/Mo-*n* (a), N_2 adsorption/desorption isotherms of various Si/Mo-*n* (b).

Table 2 Structural parameters of various Si/Mo-*n* molecular sieves

Sample	Mo content[a] (wt%)	S_{BET}[b] (m^2 g^{-1})	V_{micro}[c] (cm^3 g^{-1})	V_{meso}[c] (cm^3 g^{-1})	V_{total}[d] (cm^3 g^{-1})
Silicate-1	—	382.4	0.1606	0.0964	0.2574
Si/Mo-100	0.32	315.6	0.1371	0.0809	0.2183
Si/Mo-50	0.54	320.8	0.1404	0.0656	0.2057
Si/Mo-33	0.67	321.1	0.1400	0.0730	0.2125
Si/Mo-25	0.99	313.9	0.1369	0.0721	0.2091

[a] Determined by ICP-OES. [b] S_{BET} of the sample was calculated by the BET method. [c] Calculation of V_{micro} by HK method. [d] Calculation of V_{meso} by BJH method.

the UV-vis spectrum is usually attributed to the presence of isolated Mo^{6+} species,[38] indicating that a part of Mo species has entered the skeleton of the MFI-type molecular sieve.[38,39] The absorption peak at 265 nm, which can be attributed to the electronic leap of the Mo–O–Mo bridge bond in the oligomeric molybdenum oxide species,[40] the results confirmed again that MoO_3 species presence in the Si/Mo-*n*.

Besides the textural property, the acid amount of the catalyst greatly influences the catalytic performance, and metal modification is considered an effective measure to adjust the acidic sites of the molecular sieve.[14] NH_3-TPD was used to analyze the distribution of acidity in the catalyst, the desorption peaks of NH_3 at lower temperatures (100–300 °C) and higher temperatures (300–600 °C) correspond to the weakly acidic sites and strongly acidic sites of the molecular sieve respectively (Fig. 6). Weakly acidic sites mainly originate from non-framework molybdenum or silanol groups on the surface of the molecular sieves, while strongly acidic sites mainly originate from framework-coordinated molybdenum.[30] As listed in Table 3, total acidity increases with Mo

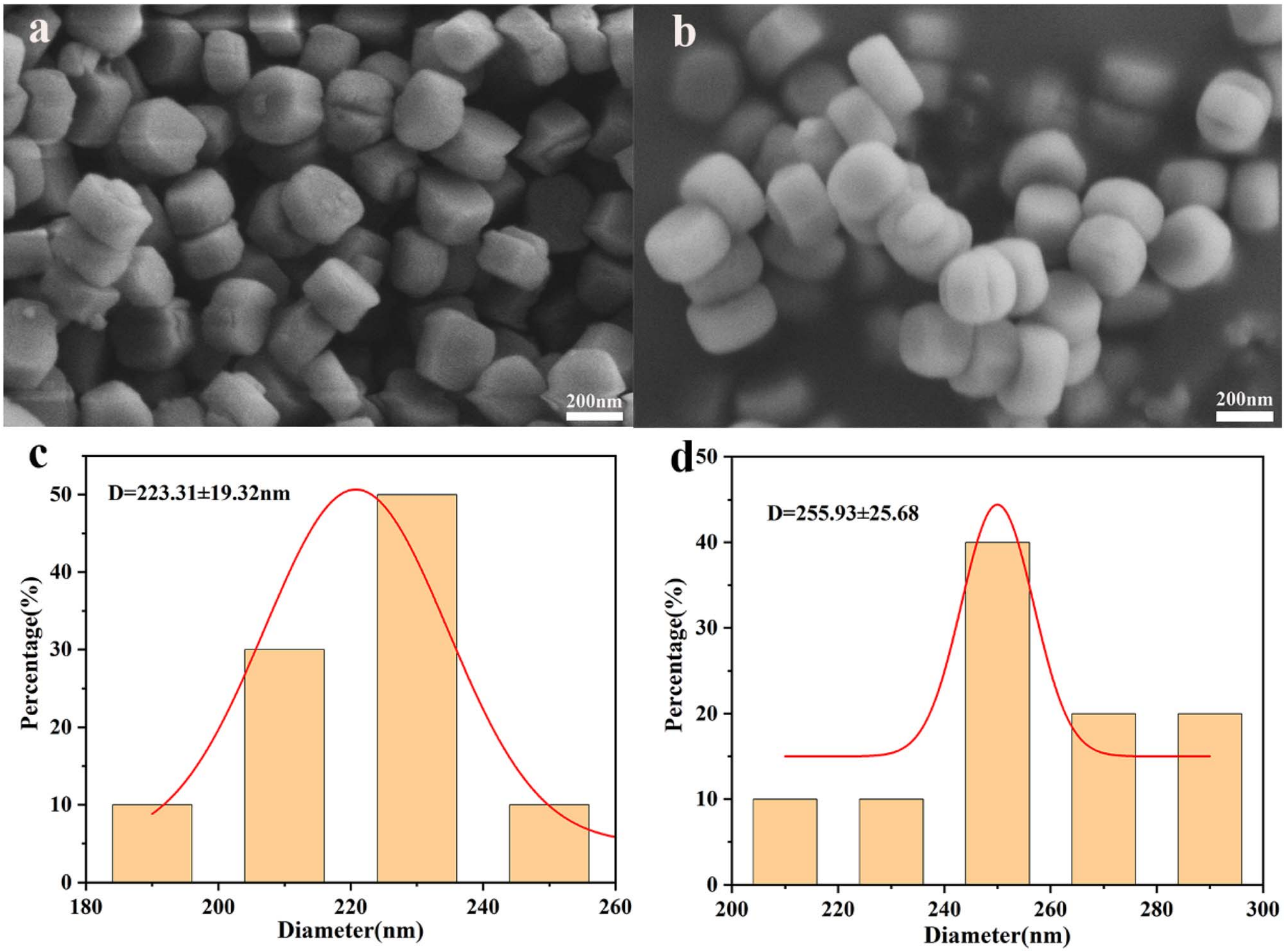

Fig. 3 Scanning electron microscope image of Silicate-1 (a), scanning electron microscope image of Si/Mo-33 (b), particle size distribution of Silicate-1 (c), particle size distribution of Si/Mo-33 (d).

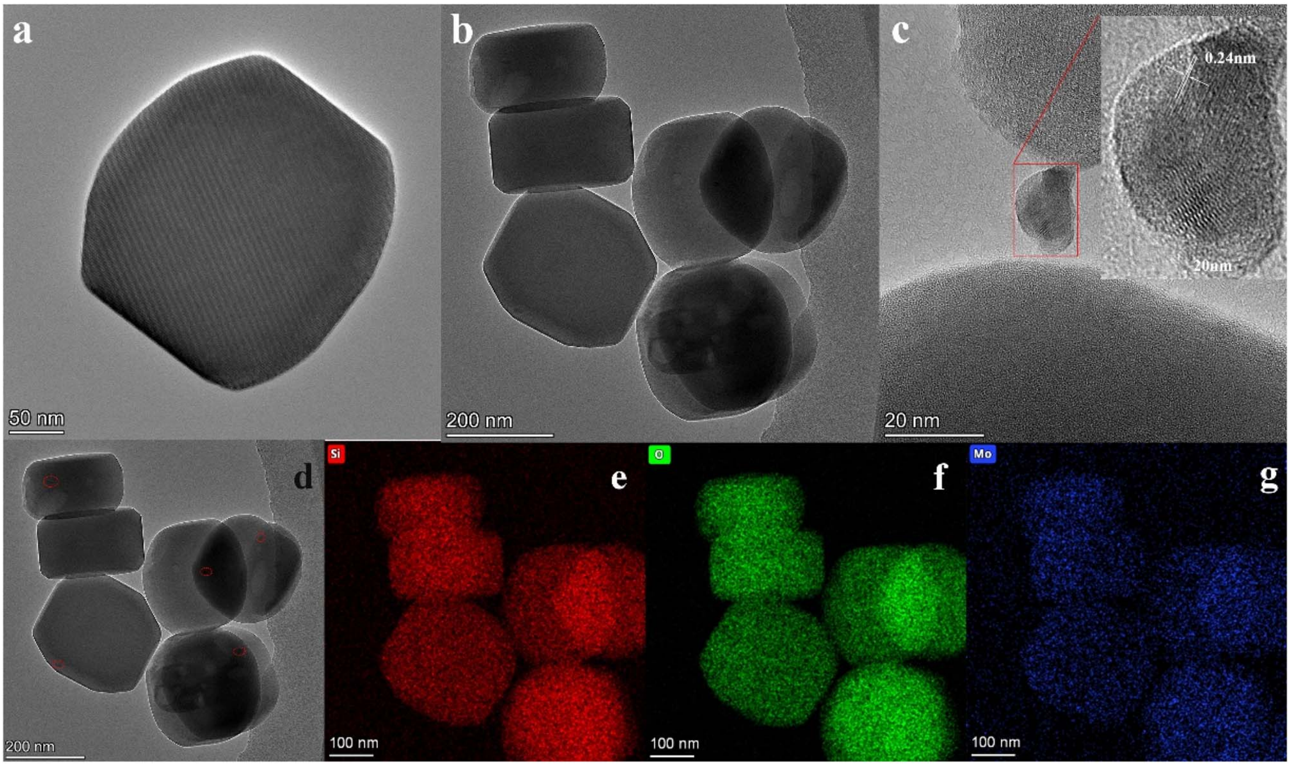

Fig. 4 Transmission electron microscopy images of Silicate-1 (a), Si/Mo-33 (b–d), Si/Mo-33 (d) corresponding composition analysis (e–g): Si (red), O (green), Mo (blue).

content. It is noteworthy that the slightly lower weak acidity of Si/Mo-33 compared to Si/Mo-50 is probably due to the potential point defect in Si/Mo-50 that prevents the formation of silanols by saturating the oxygen bridge with Mo atom coordination.[30] Meanwhile, the strong acidity increases from 0.097 mmol g^{-1} to 0.133 mmol g^{-1}, which is attributed to the framework-coordinated molybdenum.

3.2 Product analysis

3.2.1 Effect of corn stover addition on the yield of pyrolysis products. The pyrolysis product yields at different corn stover ratios are shown in Fig. 7. In general, the pyrolysis liquid products of coal and biomass consist mainly of tar and water, where the tar products are mainly derived from the condensates in the volatile fractions of coal and biomass pyrolysis. The water is mainly from

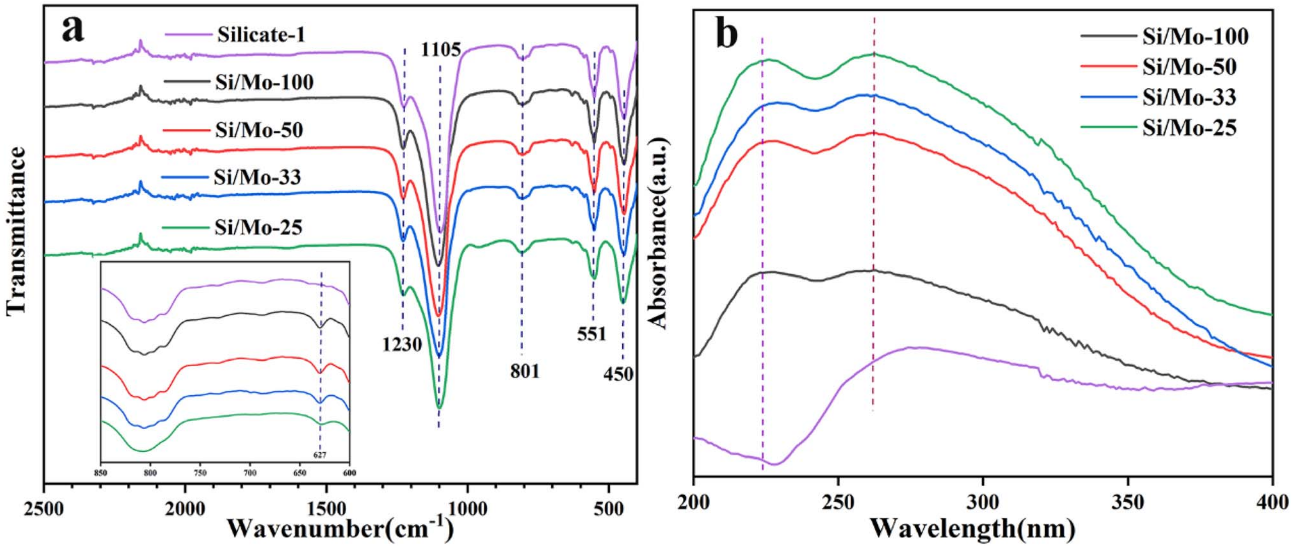

Fig. 5 FT-IR spectra of various Si/Mo-*n* (a), UV-vis spectra of various Si/Mo-*n* (b).

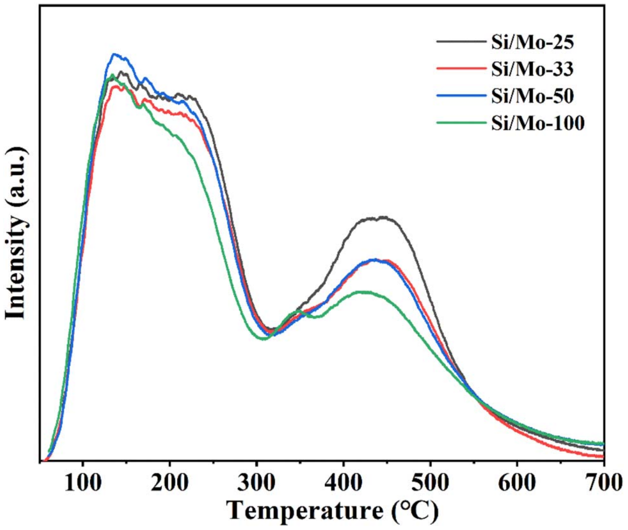

Fig. 6 NH_3-TPD plots of various Si/Mo-*n*.

Table 3 Acidity distribution of various Si/Mo-*n*

Sample	Weak acid (mmol g^{-1})	Strong acid (mmol g^{-1})	Total (mmol g^{-1})
Si/Mo-25	0.193	0.133	0.326
Si/Mo-33	0.181	0.113	0.294
Si/Mo-50	0.183	0.107	0.290
Si/Mo-100	0.163	0.097	0.260

the residual bound water in coal and biomass, and the dehydration of oxygenated compounds during pyrolysis.[23] As shown in Fig. 7a, with the increase of corn stover amount, the solid product yield decreased from 72.6 wt% to 60.2 wt%, the gas product yield showed a fluctuating trend, and the yield of liquid products increased and then decreased, while the highest yield of liquid products was achieved at 22.6 wt% with the addition of 30 wt% corn stover. Notably, the yield of tar also reached its highest value of 11.4 wt% at this point (Fig. 7b). It might be attributed to the H/C ratio of corn stover being higher than that of low metamorphic coal, and when a small amount of corn stover is added, a large amount of H/OH radicals are generated in the early pyrolysis process, and these radicals act as hydrogen donors in the subsequent pyrolysis of low metamorphic coal to promote the pyrolysis processes.[9] When the addition of corn stover exceeds 30 wt%, the tar yield gradually decreases. This may be due to the excessive corn stover and its pyrolytic coke covering the surface of the coal, which hinders the volatiles overflow and weakens or even inhibits the pyrolysis of the coal.[24] As shown in Fig. 7b, the yield of pyrolysis water also shows a trend of increasing and then decreasing, and the pyrolysis water yield decreased as the addition of corn stover above 40 wt%, which may be due to the formation of phenolic compounds from aromatic radicals generated by coal pyrolysis and OH radicals generated by corn stover pyrolysis, thus inhibiting the generation of pyrolysis water.[25] Therefore, in the subsequent study, 30 wt% of corn stover was chosen as the optimal ratio.

3.2.2 Effect of catalyst on pyrolysis product yield distribution. The yield distribution of the co-pyrolysis product after the addition of the catalyst is shown in Fig. 8, which shows that the catalyst does not affect the char of co-pyrolysis because the samples are placed in layers with the catalyst. Compared to non-catalytic pyrolysis, gas yield increased while tar and water yield decreased in the presence of the catalyst. This was attributed to the catalyst's strong acid sites and pore structure, which led to the secondary cracking of the primary volatiles. The secondary cracked small molecules will undergo aromatization and cyclization, generating large quantities of gas in the pores of the molecular sieve, thus reducing the tar yield whilst improving the quality of the tar.[25] In various catalytic pyrolysis processes, the catalytic pyrolysis tar yield reached a maximum of 9.8% at Si/Mo-33, probably due to the suitable acidity and adapted pore structure of the Si/Mo-33 catalyst. However, the tar yield was decreased at

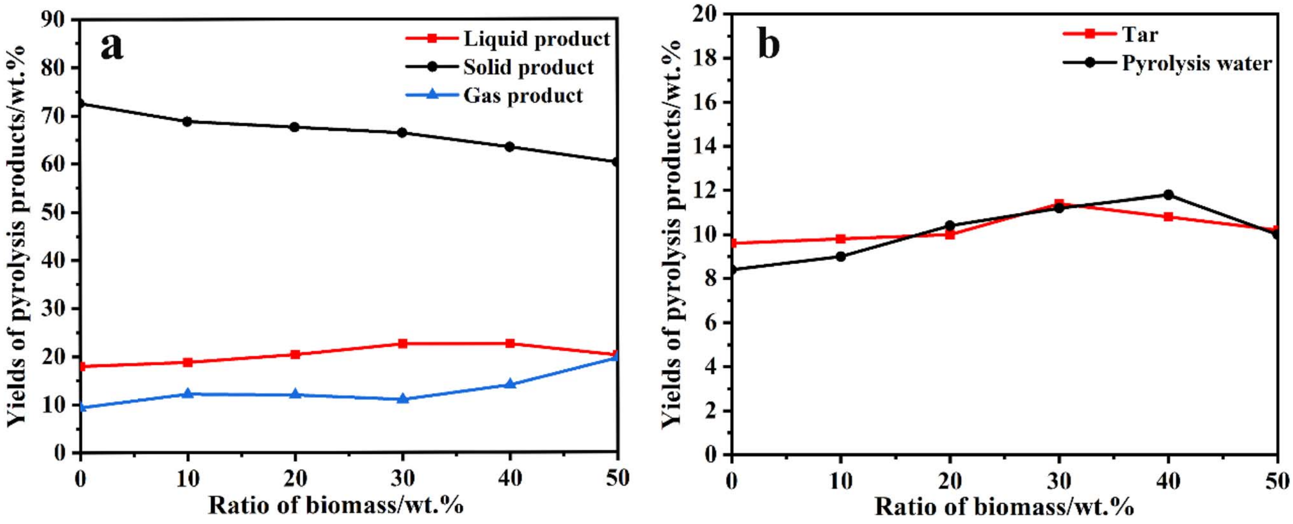

Fig. 7 Pyrolysis product yields (a) and liquid product yield (b) at different corn stover ratios.

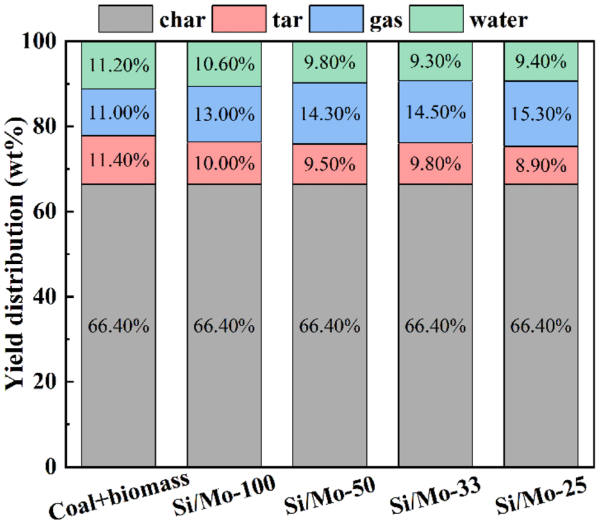

Fig. 8 Catalytic pyrolysis product yield distribution.

the Si/Mo-25 with the highest strong acidity, indicating that although the strong acid sites facilitate cracking, it leads to increased carbon deposition build-up to affect tar yield.

3.2.3 Effect of catalyst addition on the fraction of pyrolysis products. The fractions of tar were analyzed using GC-MS, and the characteristic peaks of the fractions are illustrated in Fig. 9a. The pyrolysis tar fraction of pure coal was mainly concentrated after 20 minutes in the spectrum of GC-MS. Compared to pure coal, the characteristic peaks of the tar fraction from the coal and biomass co-pyrolysis became flatter, and the content of the tar fraction slightly increased before 20 minutes. After the addition of the catalyst, the peaks associated with the tar fraction shifted towards shorter retention times, and a majority of peaks appeared within the range of 10–20 min. Among all of the catalytic tar samples, the Si/Mo-33 catalyst had the most significant catalytic effect, with the highest peak intensity and largest relative peak area of tar fraction at lower retention times in GC-MS.

For a more visual representation of the catalytic effect, we classified the tar into light oil, intermediate oil, and heavy oil according to the number of carbon atoms.[26,27] The results indicate that the light oil, intermediate oil, and heavy oil contents in the co-pyrolysis tar were 62.58%, 23.36%, and 14.06%, respectively, under the action of Si/Mo-33 catalyst (Fig. 9b). Specifically, the light oil content of catalytic co-pyrolysis was 126% higher than that of co-pyrolysis and 169% higher than that of pure coal pyrolysis. These results indicate that the Si/Mo-33 catalyst significantly increased the content of light oil in tar. It is attributed to the lower pyrolysis stability of long-chain alkanes, which are easier to decompose into low-molecular alkanes and alkenes in the catalytic pyrolysis process, thus significantly improving the quality of tar.[28]

Fig. 10a demonstrates that the inclusion of biomass led to a noteworthy reduction in hydrocarbon compounds and a rise in phenolic substances in the co-pyrolysis tar. Under the effect of Si/Mo-33 catalysis, the hydrocarbon content was reduced to a minimum and the phenolic content reached a maximum. This change can be attributed to the pyrolysis volatilities of biomass catalyzed by a molecular sieve to produce a large number of H/OH free radicals, which are more favorable to react with polycyclic aromatic hydrocarbons and aliphatic hydrocarbons produced by coal pyrolysis. Fig. 10b reveals that the prepared catalysts exhibit high selectivity in the synthesis of phenolics, particularly the low-level phenols. The Si/Mo-33 increased the phenol content in co-pyrolysis tar from 4.91% to 11.48%, a significant improvement of 133.8%. Additionally, the catalyst was able to increase cresol content by 112.2% and xylenol content by 88.1%.

3.3 Proposed pathway for catalytic upgrade

In summary, the metal loading can effectively improve the composite molecular sieve's pore structure and acid site distribution to enhance the catalytic performance. Based on the increase of phenolics and significant reduction of hydrocarbons in co-pyrolysis tar fractions, a possible conversion pathway of Mo-MFI molecular sieves to promote the lightweight of coal-biomass co-pyrolysis tar is proposed in Fig. 11.

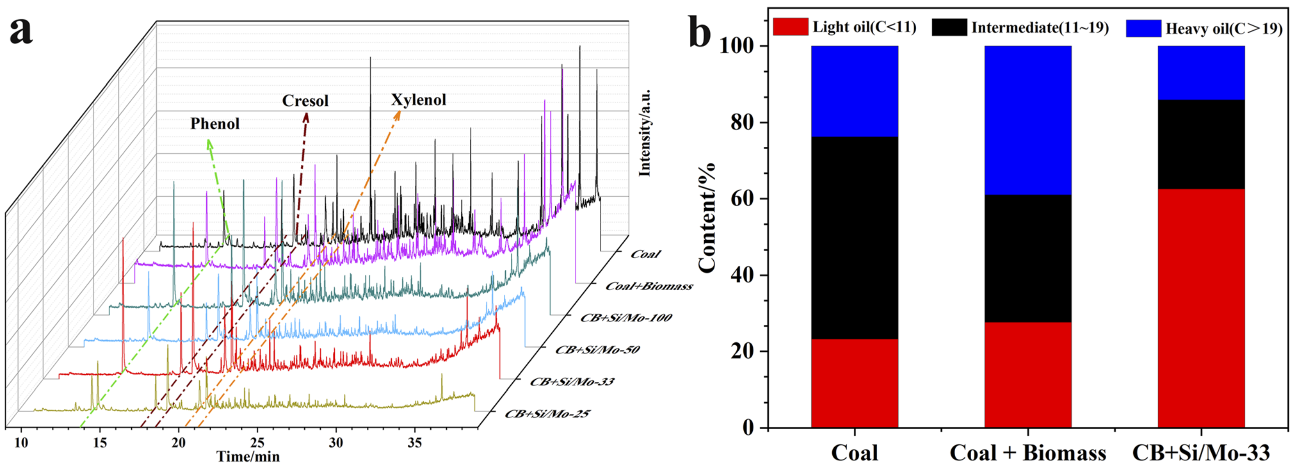

Fig. 9 GC-MS spectrum of pyrolysis tar (a); content of light, medium and heavy oil in tar samples (b).

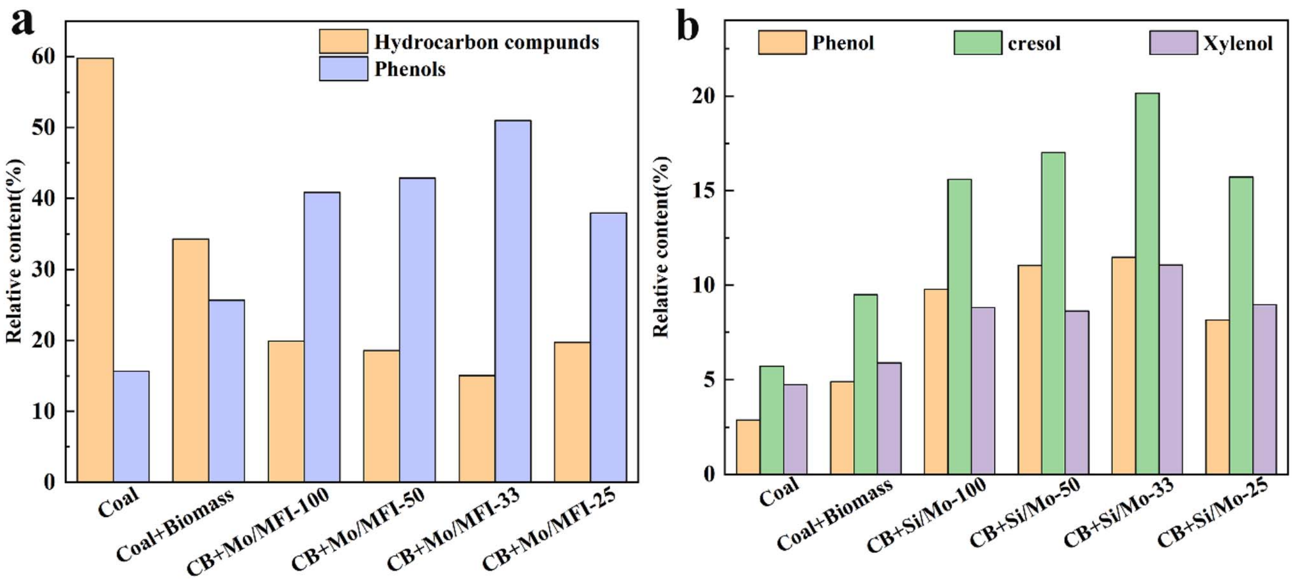

Fig. 10 Content of hydrocarbons and phenols in pyrolysis tar (a); content of low-level phenols (phenol, cresol, xylenol) in pyrolysis tar (b).

In this catalytic system, the doping of metal Mo increases the strong acid sites of MFI molecular sieves, which are the main active centers where the cracking reaction of long-chain aliphatic and aromatic alkyl side chains. The carbon chains break at acidic centers *via* a carbon-positive ion (C^+) mechanism, resulting in the formation of short-chain hydrocarbons and hydrogen species and these hydrogen species can act as a source of H in the overall catalytic system. Furthermore, the Mo-MFI acid center promotes hydrogen transfer to stabilize macromolecular radicals during coal pyrolysis, inhibiting intermolecular aggregation and increasing lighter components. The depletion of hydrogen species further promotes the conversion of long-chain aliphatic and aromatic hydrocarbons.[41] Short-chain alkanes can be aromatized with the participation of molybdenum species (skeletal Mo and non-skeletal MoO_3).[42,43]

During the co-pyrolysis of coal and biomass, the biomass decomposes at a lower temperature than the coal. As a result, it interacts preferentially with the catalyst to produce reactive radicals (OH radicals). These radicals induce hydroxyl addition reactions of monocyclic aromatic hydrocarbons, thus enhancing the content of low-level phenols and achieving the enrichment of high-value-added products.

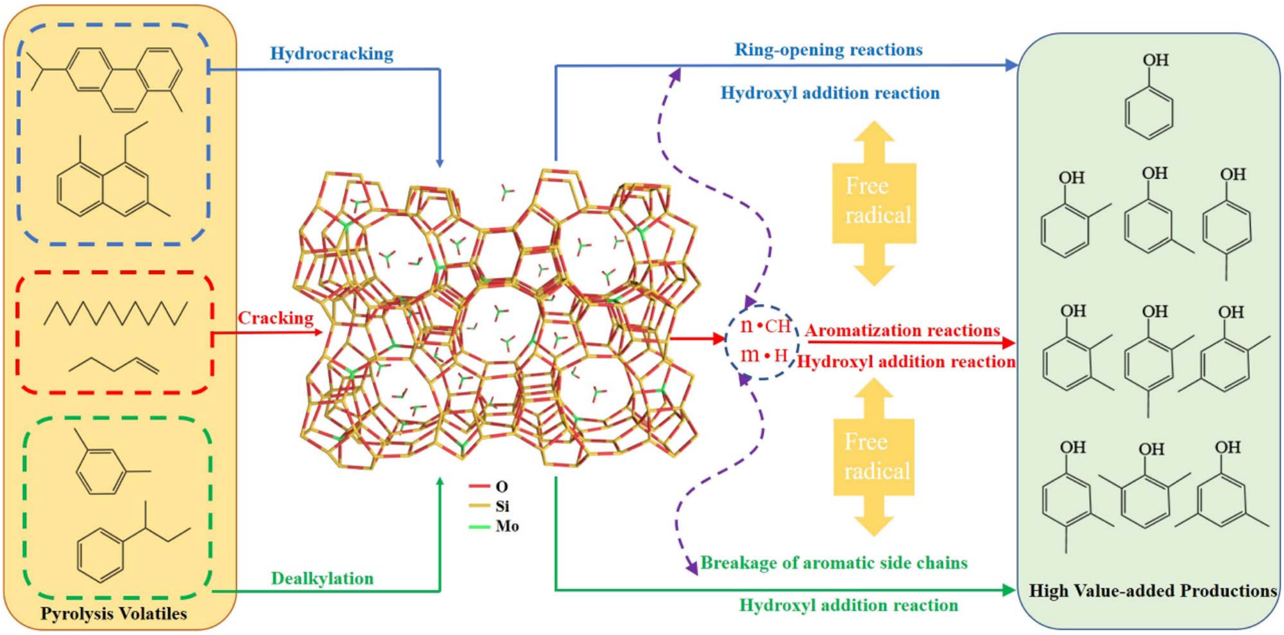

Fig. 11 Catalytic quality enhancement pathway of volatile fraction from co-pyrolysis of coal and biomass over Mo-MFI catalyst.

4. Conclusion

To improve the quality of tar, the enrichment of high-value-added products in co-pyrolysis tar was achieved with the help of biomass and catalyst. During the synthesis of the catalyst, Mo-MFI molecular sieves with varying silicon-to-molybdenum ratios were successfully synthesized by adding transition-metal Mo with TPAOH as the structural guide. The Mo-MFI zeolite catalysts were characterized using various techniques, and results showed that the Si/Mo-33 catalyst was the best for catalytic reforming due to its large specific surface area (321.1 $m^2 g^{-1}$) and suitable acidity (0.294 mmol g^{-1}). Compared with the co-pyrolysis tar product, the Si/Mo-33 enhanced the light oil content of co-pyrolysis tar by 126%, and the content of phenol, cresol, and xylenol by 133.8%, 112.2%, and 88.1%, respectively. This work is significant for enriching high-value-added products in tar and utilizing biomass resources.

Author contributions

Qiuli Zhang: revision, supervision, funding acquisition. Shuo Zhang: research, experimental conducting, discussion, writing-original draft. Junli Liu: discussion, supervision. Zhongyi Ning, Jingjing Li, and Jiahui Liu: experimental conducting. Jun Zhou and Lei Wu: revision, supervision.

Conflicts of interest

The authors declare that they have no known competing financial interests or personal relationships that could have appeared to influence the work reported in this paper.

Acknowledgements

The authors would like to acknowledge the support of the Innovation Capability Support Program of Shaanxi (Program No. 2020TD-028), the Natural Science Basic Research Program of Shaanxi (Program No. 2019JLP-17).

References

1 Y. P. Zhao, H. Q. Hu, L. J. Jin, X. F. He and S. W. Zhu, Pyrolysis Behavior of Macerals from Weakly Reductive Coals, *Energy Fuels*, 2010, **24**, 6314–6320.

2 Y. Zhang, Z. W. Yuan, M. Margni, C. Bulle, H. Hua, S. Y. Jiang and X. W. Liu, Intensive carbon dioxide emission of coal chemical industry in China, *Appl. Energy*, 2019, **236**, 540–550.

3 C. F. Yao, Y. C. Hou, S. H. Ren, W. Z. Wu, K. Zhang and Y. A. Ji, Efficient separation of phenol from model oils using environmentally benign quaternary ammonium-based zwitterions *via* forming deep eutectic solvents, *Chem. Eng. J.*, 2017, **326**, 620–626.

4 Z. W. Ge, L. J. Guo and H. Jin, Catalytic supercritical water gasification mechanism of coal, *Int. J. Hydrogen Energy*, 2020, **45**, 9504–9511.

5 T. L. Liu, F. Ning, Q. Li, Z. H. Li and X. Y. Zhao, Post-synthesis of HZSM-5 by aluminum fluoride in an acidic fluoride solution for enhanced reforming of lignite pyrolytic volatiles into light aromatics, *Energy Fuels*, 2023, **37**, 10929–10938.

6 F. Q. Guo, X. M. Zhao, K. Y. Peng, S. Liang, X. P. Jia and L. Qian, Catalytic reforming of biomass primary tar from pyrolysis over waste steel slag based catalysts, *Int. J. Hydrogen Energy*, 2019, **44**, 16224–16233.

7 G. L. Li, L. J. Yan and R. F. Zhao, Improving aromatic hydrocarbons yield from coal pyrolysis volatile products over HZSM-5 and Mo-modified HZSM-5, *Fuel*, 2014, **130**, 154–159.

8 J. T. Wei, M. Wang, F. C. Wang, X. D. Song, G. S. Yu, Y. R. Liu, J. Xu and S. Zhang, A review on reactivity characteristics and synergy behavior of biomass and coal Co-gasification, *Int. J. Hydrogen Energy*, 2021, **46**, 17116–17132.

9 Z. B. Laougé and M. Hasan, Investigation of thermal behavior of pine sawdust and coal during co-pyrolysis and co-combustion, *Energy*, 2021, **231**, 120895.

10 X. G. Huo, X. G. Jia, C. Z. Song, F. Yun, S. G. Hao, Y. Q. Ding, S. Q. Liu and M. Z. Lei, Investigation of mitigation of nitric oxide emission characteristics and slagging properties from biomass combustion by the additive of coal gangue, *J. Environ. Chem. Eng.*, 2022, **10**, 107573.

11 G. T. Kokotailo, S. L. Lawton, G. T. Olson and W. M. Meier, Structure of Synthetic Zeolite ZSM-5, *Nature*, 1978, **272**, 437–438.

12 R. Y. Wang, C. J. Xia and B. Peng, Fundamental understanding and catalytic applications of hollow MFI-type zeolites, *Catal. Today*, 2022, **405**, 111–124.

13 J. Grand, S. N. Talapaneni, A. Vicente, C. Fernandez, E. Dib and H. A. Aleksandrov, One-Pot Synthesis of Silanol-Free Nanosized MFI Zeolite, *Nat. Mater.*, 2017, **16**, 1010–1015.

14 C. Y. Bi, Z. Z. Zhang, D. Z. Han, C. G. Wang, J. B. Zhang and X. X. Ma, Effective regulation of Ga active species in mesoporous ZSM-5 for catalytic upgrading of coal pyrolysis volatiles, *Fuel*, 2022, **321**, 124105.

15 Z. X. Yang, K. Ajay and A. Allen, Integration of biomass catalytic pyrolysis and methane aromatization over Mo/HZSM-5, *J. Anal. Appl. Pyrolysis*, 2016, **120**, 484–492.

16 L. Jin, X. Zhou, X. He and H. Hu, Integrated coal pyrolysis with methane aromatization over Mo/HZSM-5 for improving tar yield, *Fuel*, 2013, **114**, 187–190.

17 L. Qi, C. Peng, Z. M. Cheng and Z. M. Zhou, Structure-performance relationship of NiMo/Al_2O_3-HY catalysts in selective hydrocracking of poly-aromatics to mono-aromatics, *Chem. Eng. Sci.*, 2022, **263**, 118121.

18 P. Wehrer, L. Hilaire and G. Maire, About the stability of alkane isomerizing catalysts made up of molybdenum oxides, *Appl. Catal., A*, 2001, **208**, 259–264.

19 Y. P. Ban, L. J. Jin, K. C. Wang, Y. Li, H. Yang and H. Q. Hu, Catalytic effect of industrial waste carbide slag on pyrolysis of low-rank coal, *Energy*, 2023, **265**, 126368.

20 J. P. Zhao, J. P. Cao, H. Xiang, F. Wei, N. Y. Yao, F. Chen and X. B. Pang, Catalytic Upgrading of Lignite Pyrolysis Volatiles to Aromatics over Urea-Modified HZSM-5: Study on Desilication of Preserved Micropores, *Energy Fuels*, 2023, **37**, 6515–6523.

21 M. B. Folgueras, D. R. María and J. Xiberta, Pyrolysis of blends of different types of sewage sludge with one bituminous coal, *Energy*, 2005, **30**, 1079–1091.

22 D. L. Wang, Z. H. Chen, J. Yu and S. Q. Gao, Effect of Si/Al ratio of HZSM-5 zeolites on catalytic upgrading of coal pyrolysis volatiles, *J. Fuel Chem. Technol.*, 2021, **49**, 634–641.

23 G. Zhou, P. A. Jensen, D. M. Le, N. O. Knudsen and A. D. Jensen, Direct upgrading of fast pyrolysis lignin vapor over the HZSM-5 catalyst, *Green Chem.*, 2016, **18**, 1965–1975.

24 L. Wu, J. Liu, P. Xu, J. Zhou and F. Yang, Biomass hydrogen donor assisted microwave pyrolysis of low-rank pulverized coal: optimization, product upgrade, and synergistic mechanism, *Waste Manage.*, 2022, **143**, 177–185.

25 B. Tian, W. Y. Zhao, Q. J. Guo and Y. Y. Tian, A comprehensive understanding of the synergetic effect and volatile interaction mechanisms during co-pyrolysis of rice husk and different rank coals, *Energy*, 2022, **254**, 124388.

26 H. Y. Zhao, Y. H. Li, Q. Song, S. C. Liu, J. Yan, Q. X. Ma, L. Ma and X. Q. Shu, Investigation on the thermal behavior characteristics and products composition of four pulverized coals: its potential applications in coal cleaning, *Int. J. Hydrogen Energy*, 2019, **44**, 23620–23638.

27 M. Sun, D. Zhang, Q. X. Yao, Y. Q. Liu, X. P. Su and J. Charles, Separation and composition analysis of GC/MS analyzable and unanalyzable parts from coal tar, *Energy Fuels*, 2018, **32**, 7404–7411.

28 X. J. Jin, J. H. Lee and J. W. Choi, Catalytic co-pyrolysis of woody biomass with waste plastics: effects of HZSM-5 and pyrolysis temperature on producing high-value pyrolytic products and reducing wax formation, *Energy*, 2022, **239**, 121739.

29 T. Zhang, Y. Zuo, M. Liu, C. S. Song and X. W. Guo, Synthesis of Titanium Silicalite-1 with High Catalytic Performance for 1-Butene Epoxidation by Eliminating the Extraframework Ti, *ACS Omega*, 2016, **1**, 1034–1040.

30 F. Dubray, S. Moldovan, C. Kouvatas, J. Grand, C. Aquino and N. Barrier, Direct Evidence for Single Molybdenum Atoms Incorporated in the Framework of MFI Zeolite Nanocrystals, *J. Am. Chem. Soc.*, 2019, **141**, 8689–8693.

31 G. Ye, L. L. Wan, Q. L. Zhang, H. Liu, J. Zhou and L. Wu, Boosting Catalytic Performance of MOF-808(Zr) by Direct Generation of Rich Defective Zr Nodes *via* a Solvent-Free Approach, *Inorg. Chem.*, 2023, **10**, 4248–4259.

32 G. Ye, H. L. Wang, W. X. Chen, H. Q. Chu, J. S. Wei and D. G. Wang, *In Situ* Implanting of Single Tungsten Sites into Defective UiO-66(Zr) by Solvent-Free Route for Efficient Oxidative Desulfurization at Room Temperature, *Angew. Chem., Int. Ed.*, 2021, **60**, 20318–20324.

33 G. J. Yang, J. Han, Z. Y. Qiu, X. X. Chen, Z. C. Feng and J. H. Yu, An amino acid-assisted approach to fabricate nanosized hierarchical TS-1 zeolites for efficient oxidative desulfurization, *Inorg. Chem. Front.*, 2020, **7**, 1975–1980.

34 C. Bi, X. U. Wang, Q. You, B. Liu, Z. Li and J. Zhang, Catalytic upgrading of coal pyrolysis volatiles by Ga-substituted mesoporous ZSM-5, *Fuel*, 2020, **267**, 117217.

35 Q. Y. Xi, J. S. Liu, Z. Y. Wu, H. F. Bi, Z. Q. Li and K. J. Zhu, In-Situ Fabrication of MoO_3 Nanobelts Decorated with MoO_2 Nanoparticles and Their Enhanced Photocatalytic Performance, *Appl. Surf. Sci.*, 2019, **480**, 427–437.

36 S. T. Du, Q. M. Sun, N. Wang, X. X. Chen, M. J. Jia and J. H. Yu, Synthesis of Hierarchical TS-1 Zeolites with Abundant and Uniform Intracrystalline Mesopores and Their Highly Efficient Catalytic Performance for Oxidation Desulfurization, *J. Mater. Chem. A*, 2017, **5**, 7992–7998.

37 S. W. Li, W. Wang and J. S. Zhao, Catalytic Oxidation of DBT for Ultra-Deep Desulfurization Under MoO_3 Modified Magnetic Catalyst: The Comparison Influence on Various Morphologies of MoO_3, *Appl. Catal., A*, 2020, **602**, 117671.

38 Z. R. Zhang, J. S. Suo and X. M. Zhang, Characterization and Catalytic Testing of W-MCM-41 Mesoporous Molecular Sieves, *Appl. Catal., A*, 1999, **179**, 11–19.

39 X. L. Zhang, C. Y. Yuan, M. Y. Li, B. Gao, X. Y. Wang and X. C. Zheng, Synthesis and Characterization of Mesoporous, Tungsten-Containing Molecular Sieve Composites, *J. Non-Cryst. Solids*, 2009, **355**, 2209–2215.

40 J. Luo, W. Q. Liu, J. Xiong, L. Yang, H. P. Li and S. Yin, SBA-15 Supported Molybdenum Oxide Towards Efficient Catalytic Oxidative Desulfurization: Effect of Calcination Temperature of Catalysts, *J. Chin. Adv. Mater. Soc.*, 2018, **6**, 44–54.

41 X. Gao, Z. Zhou, J. W. Wang, H. Tian, M. X. Qing and L. Y. Jiang, Comparative study of the catalytic co-pyrolysis of microalgae (*Chlorella vulgaris*) and polypropylene with acid and base catalysts toward valuable chemicals production, *Fuel Process. Technol.*, 2023, **241**, 107520.

42 Y. R. Park, G. H. Han, S. Y. Kim, D. H. Kim, Y. G. Hur and K. Y. Lee, Cooperative catalysis of Co-promoted Zn/HZSM-5 catalysts for ethane dehydroaromatization, *Fuel*, 2023, **349**, 128583.

43 D. H. Zeng, G. L. Zhu and C. G. Xia, Recent advances of aromatization catalysts for C_4 hydrocarbons, *Fuel Process. Technol.*, 2022, **226**, 107087.